Journal of Membrane Science 607 (2020) 118139

Contents lists available at ScienceDirect

Journal of Membrane Science

journal homepage: http://www.elsevier.com/locate/memsci

A fouling-resistant mixed-matrix nanofiltration membrane based on covalently cross-linked $Ti_3C_2T_X$ (MXene)/cellulose acetate

Ravi P. Pandey [a], P. Abdul Rasheed [a], Tricia Gomez [a], Reem S. Azam [a,b], Khaled A. Mahmoud [a,*]

[a] Qatar Environment and Energy Research Institute (QEERI), Hamad Bin Khalifa University (HBKU), P.O. Box 34110, Doha, Qatar
[b] Materials Science and Technology Program, College of Arts and Sciences, Qatar University, Doha, 2713, Qatar

ARTICLE INFO

Keywords:
$Ti_3C_2T_X$ MXene
Cellulose acetate
Mixed-matrix
Nanofiltration membrane
Antifouling

ABSTRACT

A new fouling-resistant mixed-matrix nanofiltration membrane based on a covalently cross-linked $Ti_3C_2T_X$ (MXene)/cellulose acetate (MXene@CA) composite was fabricated by phase inversion followed by formaldehyde cross-linking. The physicochemical properties of the prepared MXene@CA composite membranes were studied by field emission scanning electron microscopy (FESEM), energy dispersive spectroscopy (EDS), X-ray diffraction (XRD), and water contact angle techniques. The performance of the prepared membranes was evaluated with respect to the water flux, bacterial growth inhibition, and rejection properties. The 10%MXene@CA (10:90 wt % of MXene:CA) composite membrane shows high pure water flux of ~256.85 L m^{-2} h^{-1} bar^{-1}, 123.28% water uptake, and 69.7% porosity. The 10%MXene@CA membrane, exhibited more than 92% and 98% rejection of rhodamine B (RhB) and methyl green (MG), respectively. Furthermore, 10%MXene@CA membrane exhibited more than 98% and 96% growth inhibition for *E. coli* and *B. subtilis*, respectively. Also, the optimal membrane showed a significantly improved hydrophilicity (water contact angle = 60.8°), which has favored good antifouling properties. The reported nanofiltration membrane, especially 10%MXene@CA, can be suggested for water purification and biomedical applications.

1. Introduction

Nowadays, nanofiltration (NF) has become one of the cutting-edge pressure-driven membrane separation techniques used for water softening, wastewater treatment, chemical, and pharmaceutical industries, etc. [1–4]. NF has been efficiently used in the selective rejection of multivalent ions and charged organic molecules due to their unique separation mechanisms such as steric hindrance and Donnan exclusion [3,5,6]. High selectivity, (chemical and mechanical) stability, and fouling resistance are crucial criteria for developing functional NF membranes [1,7–11]. To minimize fouling and improve the properties of NF membranes various strategies have been proposed such as modification with highly hydrophilic polymers [12–14], and incorporation of nanomaterials [15,16]. Among these strategies, incorporation of hydrophilic nanomaterials into polymeric membranes leads to tremendous enhancement of the membrane stability, hydrophilicity and antifouling properties [17–20]. However, mixed-matrix hybrid membranes prepared by physical blending can agglomerate or leach out, thus possible loss to homogeneity, which might decrease the membrane separation performance [21].

Among other hydrophilic polymers being used to fabricate NF membranes [22–25], cellulose acetate (CA) was considered as a promising alternative because of their good water affinity, biodegradability, excellent film-forming capability, high toughness, hydrophilic, excellent biocompatibility, easy chemical modification, and relatively low cost [26–28]. However, CA membranes are highly susceptible to fouling by biological and organic contaminants leads to deterioration in its overall separation performances [29,30]. These challenges encouraged researchers to improve the antifouling properties of CA membranes by the incorporation of nanomaterials, especially 2D nanosheets, to achieve improved separation performances [29–32].

Recently, the 2D MXenes have attracted extensive attention for diverse applications including water treatment membranes, due to their excellent flexibility, mechanical stability, chemical tunability, hydrophilic surfaces, and most significantly their nanometer thin 2D structure with excellent antibacterial activity [33–38]. Particularly, $Ti_3C_2T_x$ has been the most explored MXene for various applications such as efficient removal of ions, heavy metals, dyes, and radionuclides [39–41]. $Ti_3C_2T_X$ is typically prepared by selective etching of the Al layer from MAX (Ti_3AlC_2) through either direct HF etching or *in situ* HCl/LiF acid

* Corresponding author.
E-mail address: kmahmoud@hbku.edu.qa (K.A. Mahmoud).

https://doi.org/10.1016/j.memsci.2020.118139
Received 9 March 2020; Accepted 2 April 2020
Available online 16 April 2020

mixture [42,43]. The surface of $Ti_3C_2T_X$ is terminated by functional groups such as -O-, –OH, and/or –F [44,45]. Despite these endorsing properties, $Ti_3C_2T_x$ MXene is unable to form stable free-standing films [46]. Generally, the majority of MXene based membranes were developed based on forming a film of $Ti_3C_2T_x$ on polymeric porous support by vacuum-assisted filtration protocol [34,46–51]. Our group first time reported potential anti-microbial behavior of $Ti_3C_2T_x$ MXene and prepared water purification membranes supported on hydrophilic polyvinylidene difluoride (PVDF) substrate [38,47,49]. Wu et al. prepared solvent resistant NF membrane based on Polyacrylonitrile (PAN)/-Polyethyleneimine (PEI)-$Ti_3C_2T_x$ composite [48]. Ding et al. improved water flux of $Ti_3C_2T_x$ membrane by increasing the water transport channels, using positively charged $Fe(OH)_3$ nanoparticles as pore-forming agents [34]. $Ti_3C_2T_x$/graphene oxide (GO) composite membranes were prepared for the effective rejection of dye molecules and salts [52,53]. MXene/Polyethersulfone (PES) ultrafiltration (UF) membrane was explored for their favorable rejection of congo red [46]. Liu et al. prepared ultrathin (~60 nm thickness) $Ti_3C_2T_x$ membrane onto polyacrylonitrile support, which showed water flux 85.4 L m^{-2} h^{-1} and 99.5% rejection of NaCl at 65 °C [51]. Recently, we have reported a 21% Ag@MXene (21% loading of AgNPs) composite membrane with enhanced water flux, rejection and antifouling properties [50]. P84 copolyimide/MXene membrane showed a 100% rejection of gentian violet and flux of 268 L m^{-2} h^{-1} at 0.1 MPa [54]. Xu et al. prepared MXene/CS mixed matrix membrane for pervaporation dehydration of solvents [55].

The vast majority of $Ti_3C_2T_x$ membranes listed above, prepared by VAF on polymeric supports, have demonstrated excellent rejection and antibacterial properties of the top MXene layer. However, MXene remains weakly bound (mechanically) to the substrates, leading to easy leaching of MXene and thus declined the separation performance of overall membranes [39].

Herein, we first time prepared chemically cross-linked MXene@CA nanoporous membranes by phase inversion followed by cross-linking with formaldehyde. The performance of the prepared MXene@CA composite membranes was assessed in terms of water flux, fouling resistance, and rejection of the charged molecule.

2. Experimental section

2.1. Materials

Cellulose acetate (CA) (average Mn ~30,000 by GPC), formaldehyde, sodium chloride (NaCl), sodium sulfate (Na_2SO_4), magnesium chloride ($MgCl_2$), aluminium chloride ($AlCl_3$), lithium fluoride (LiF), Rhodamine B (RhB), bovine serum albumin (BSA), polyethylene glycol 400 (PEG-400) and methyl green (MG) were purchased from Sigma-Aldrich. Commercial Whatman CA membrane (pore size 0.2 μm) was purchased from GE healthcare Life science Germany. MAX (Ti_3AlC_2) was obtained from Y-Carbon, Ltd., Ukraine, and used as received. Other chemicals and solvents were of commercial grade and used as received.

2.2. Synthesis of delaminated MXene (DL-Ti_3C_2Tx) and cross-linked MXene@cellulose acetate (CA) based hybrid nanoporous membrane

DL-$Ti_3C_2T_x$ MXene sheets were prepared from MAX (Ti_3AlC_2) by acid (Lif/HCl) etching of the aluminum layer followed by delamination as reported earlier with some modifications [50]. Briefly, LiF (80 mg) and 1 mL of 9 M HCl were mixed in a 50 mL Teflon tube and kept under stirring, at 25 °C, for 5 min followed by the gradual addition of Ti_3AlC_2 (50 mg) and the resulting mixture was magnetically stirred for 24 h at 25 °C. The resulting mixture was centrifuged at 3500 rpm for 5 min and the solid residue was washed several times with DI water to reach a final pH $\geq$ 5.5. DL-$Ti_3C_2T_x$ was obtained by probe-sonication, under Ar (800 Watt, 30 kHz, 3/1 s on/off). The resulting solution was centrifuged at 5000 rpm for 15 min. The final DL-Ti_3C_2Tx nanosheets were obtained by freeze-drying. Cross-linked MXene@CA nanoporous membranes were developed by phase inversion followed by formaldehyde cross-linking. Typically, 0–10 wt% of DL-Ti_3C_2Tx relative to CA was dispersed in a 10 mL of acetic acid/acetone solution (1:1 ratio) using a bath sonicator. PEG-400 (0.5 g) was added into the above dispersion under stirring at 25 °C. Finally, CA (1.5 g) was added gradually under stirring at 25 °C. The resulting viscous solutions were stirred constantly followed by degassing for 24 h and cast on a glass plate using doctor blade (Labcoat Master casting system, PHILOS, Gyeonggi-do, Korea) with a thickness of 280 μm. Casted membranes were allowed to dry at room temperature (30 s) and immersed in a coagulation bath containing DI water at 15 °C for 2 h. Finally, the membranes were washed 4–5 times with DI water to remove any residual. Cross-linking of the prepared membranes were carried out using acidic formaldehyde solution (HCHO (2.5% w/v) + H_2SO_4), as reported earlier [56,57]. Briefly, the cross-linking solution was prepared by adding sodium sulfate (12 g), formaldehyde (4.328 g), and sulfuric acid (10 g) into DI water (37.6 mL) under constant stirring for 10 min at 25 °C. Prepared membranes were kept in the crosslinking solution at 60 °C for 30, 60, 90, and 120 min. Finally, cross-linked membranes were washed several times by DI water and used for further applications. Different membranes were prepared and were designated as pristine CA, cross-linked CA (CCA), non-cross-linked X% MXene/CA (X%MXene/CA), and cross-linked X%MXene@CA (X% MXene@CA), where X is the weight percentage of MXene (0–10 wt%) to CA in the membrane phase.

2.3. Characterizations

The prepared X%MXene@CA membranes were dried at 30 °C for 24 h and used for physicochemical characterizations. Fourier-transform infrared (FTIR) spectra were recorded using attenuated total reflectance (ATR) technique with a Nicolet™ iS50 FTIR Spectrometer in the range of 4000−600 cm^{-1}. The UV–vis spectra of the dye and bovine serum albumin (BSA) solutions were obtained using a Jasco V-670 absorption spectrophotometer with scan speed of 100 nm min^{-1}. Scanning electron microscopy (SEM) images were recorded by using a FEI Quanta 650 FEG SEM, after gold sputter coatings on samples. The thermal stability of MXene@CA composite membranes was studied using a thermogravimetric analyzer (TGA) (TA Instruments SDT-Q600) under a nitrogen atmosphere with 20 °C min^{-1} heating rate from 50 to 500 °C. Photographs of the prepared membrane and bacterial culture plates were taken using a Nikon digital camera (DSLR D5100). Zeta potential was measured by SurPASS Electrokinetic Analyzer (Anton Paar KG, Austria). The hydrophilicity of the prepared MXene@CA composite membranes was measured in the form of water contact angle using KRUSS Drop Shape Analyzer DSA25. Wide-angle X-ray diffractograms (WAXRDs) of MXene@CA composite membranes were recorded using a Bruker D8 Advance (Bruker AXS, Germany).

2.4. Water uptake and membrane porosity studies

Water content in the membrane phase was calculated as water uptake by measuring the weight of membrane in the dry and in the wet conditions equilibrated in DI water for 24 h. Water uptake of the prepared membranes was measured by immersing a defined square piece of the membranes in DI water for 24 h. Surficial water was removed and measured the wet weight of the membrane. The dry weight of the membranes were measured by keeping membranes under vacuum at 60 °C to get a constant weight. The water uptake (%) was calculated using Eq. (1).

$$Water\ uptake\ (\%) = \frac{W_{wet} - W_{dry}}{W_{dry}} \times 100 \quad (1)$$

where W_{dry} and W_{wet} are the weights of the dry membrane wet membrane, respectively.

In order to evaluate porosity of the membrane, known area and dry weight of membrane were kept in DI water for 24 h. The wet weight of the membrane was measured after wiping the surface water with a filter paper. Porosity of the membrane was calculated using Eq. (2):

$$Porosity\ (\%) = \left(\frac{W_{wet} - W_{dry}}{Ad\rho}\right) \quad (2)$$

where W_{wet} and W_{dry} are the wet and dry weights of the membrane, respectively. A is the membrane area, d is the thickness of membrane and ρ is the density of water.

2.5. Membrane flux, rejection, pore radius, and molecular weight cut off (MWCO) measurements

The membrane separation performance was assessed in the form of rejection and flux by filtering salts, dyes and BSA solutions, using a dead-end filtration set-up (HP4750 Stirred cell, STERLITECH, WA, USA) with an effective membrane area of about 9.60 cm^2.

The water flux (J_w) was determined by the evaluation of water permeation flow in terms of liter per squire meter per hour per bar, using the following equation:

$$J_w = V/AtP \quad (3)$$

where V is the quantity of permeation (l), A is the effective membrane surface area (m^2), t is the total time for filtration in hours, and P is the applied pressure in bar.

Aqueous solutions of different salts (NaCl, $MgCl_2$, $MgSO_4$, and Na_2SO_4) (2000 ppm), dyes (rhodamine B (RhB), and methyl green (MG)) (50, and 100 ppm) and BSA (50 and 100 ppm) were used to measure the membrane solute rejection (R) performance. The rejection (R) for solutes was expressed as follows:

$$R\ (\%) = \frac{C_f - C_p}{C_f} \times 100 \quad (4)$$

where, C_f and C_p are feed and permeate concentrations of solutes in mg/L.

Effective pore diameter (a) of developed MXene@CA composite membranes were evaluated by using Ferry equation (eq. (5)) [12].

$$R = 100\left[1 - \left(1 - r/a\right)^2\right]^2 \quad (5)$$

where, R is the solute rejection (%), and r is the solute diameter.

The MWCO of the developed membranes is expressed as the molecular weight of solutes having 90% rejection by the prepared membrane and can be calculated from the plot of rejection (%) of solute against their molecular weight in Daltons.

2.6. Membrane stabilities

Membrane oxidative stability was assessed by immersing the membrane samples in a 0.1% aqueous solution of sodium hypochlorite at 70 °C for different time (0–70 h) intervals. Membrane chemical stability was assessed in terms of percentage weight loss, using the following equation:

$$Weight\ loss\ (\%) = \frac{W_{dry} - W_{cdry}}{W_{cdry}} \times 100 \quad (6)$$

where, W_{dry} and W_{cdry} are the weight of dry and chemically treated dry membranes, respectively.

2.7. Antibacterial activity evaluation

The model gram-negative bacteria *Escherichia coli* (*E. coli*) and gram-positive bacteria *Bacillus subtilis* (*B. subtilis*) were cultured in Luria-Bertani (LB) medium at 37 °C. The bacterial cultures (*E. coli* and *B. subtilis*) were sub-cultured in LB media and harvested after 4 h by centrifugation (4500 rpm, 5 min) and the resulting residue was washed three times with phosphate-buffered saline (PBS) to obtain bacterial pellets. Obtained, bacterial pellets were diluted to an approximate cell concentration of 1×10^6 CFU mL^{-1}. The antifouling properties of CCA, 2%MXene@CA, 6%MXene@CA, 8%MXene@CA, and 10%MXene@CA membranes were evaluated against both *E. coli* and *B. subtilis* by filtering the bacterial suspensions (1×10^6 CFU mL^{-1}) through the sterilized membranes. Then, membranes were plated on LB agar and kept for incubation overnight at 37 °C. Finally, the number of colonies grown on the membrane surface was counted to quantify the bactericidal efficiency of membranes. The cell viability was calculated by the colony counting method and represented as percentage viability (%) in comparison with the control membrane (CCA). The morphology of bacterial cells on the membrane was studied by SEM, after fixing the membrane samples with glutaraldehyde (2.5%) followed by serial dehydration in ethanol solutions.

3. Results and discussion

3.1. Structural characterization of cross-linked MXene@CA nanoporous membranes

The surface functional groups (OH, -O-) make MXene highly dispersible in water and offer reactive sites for chemical crosslinking to prepare stable MXene membranes [39]. Chemically cross-linked MXene@CA composite membranes were prepared by casting the mixed matrix membrane including (0–10 wt%) DL-$Ti_3C_2T_x$ with CA followed by formaldehyde crosslinking. The detailed membrane fabrication process is given in Scheme 1. It is expected that surface-terminal groups such as –OH and –O– of MXene and –OH groups of CA react with formaldehyde and form –O–C–O– linkages [58–60]. A self-crosslinking is also expected between CA molecules. However, in our case, the content of MXene in the membrane phase is low (between 0 and 10%) and it is homogenously distributed in CA polymer matrix. Hence, it is unlikely to form self-crosslinking between MXene molecules. The FTIR spectra were conducted to trace functional groups in the prepared DL-$Ti_3C_2T_x$ and 10%MXene@CA composite membrane, respectively (Fig. S1). For DL-$Ti_3C_2T_x$, absorption peaks at ~3411 (broad band), ~1634 and ~1085 cm^{-1}, were assigned to the stretching vibration of the strongly hydrogen bonded OH group, absorbed external water and C–F group in the MXene, respectively [34]. The FTIR spectrum of 10%MXene@CA membrane shows a broad absorption band at ~3376 cm^{-1}, which is attributed to the stretching vibration of strongly hydrogen bonded OH groups of MXene and CA moieties. Characteristic peak of CA at ~1733 cm^{-1} is attributed to the C═O stretching vibration of ester groups. The absorption peaks at ~1373 and ~1229 cm^{-1} were attributed to symmetric C–H and C–O stretching vibration from CA, respectively.

Fig. 1(a&b) shows the SEM and TEM images of DL-$Ti_3C_2T_x$ that was used for membrane fabrication. SEM (Fig. 1a) evidenced successful delamination of ML-MXene stacks into wrinkled sheet-like flakes. From TEM (Fig. 1b), the single- and few-layer sheets with an average sheet size of 200–300 nm can be clearly observed.

The XRD pattern of DL-$Ti_3C_2T_x$, CA and 10%MXene@CA membranes are shown in Fig. 1 (c). Successful etching of the MAX phase was confirmed by the dimensioning of most intense Al peaks at 2θ ~9.7° and 39° [44]. Moreover, a lower angle shift and broadening of MXene characteristic peak (002) to 2θ = ~7° are characteristics of DL-$Ti_3C_2T_x$. Pristine CA shows broad peaks at ~16°, 30°, and 41° indicating the amorphous nature and non-crystalline structure. Those characteristic CA peaks were still observed in the 10%MXene@CA composite membrane together with a shift in peak (002) of MXene to lower angle at ~5.7° [44]. The interlayer spacing within the stacks of DL-$Ti_3C_2T_x$ in pristine MXene and composite 10%MXene@CA were calculated as

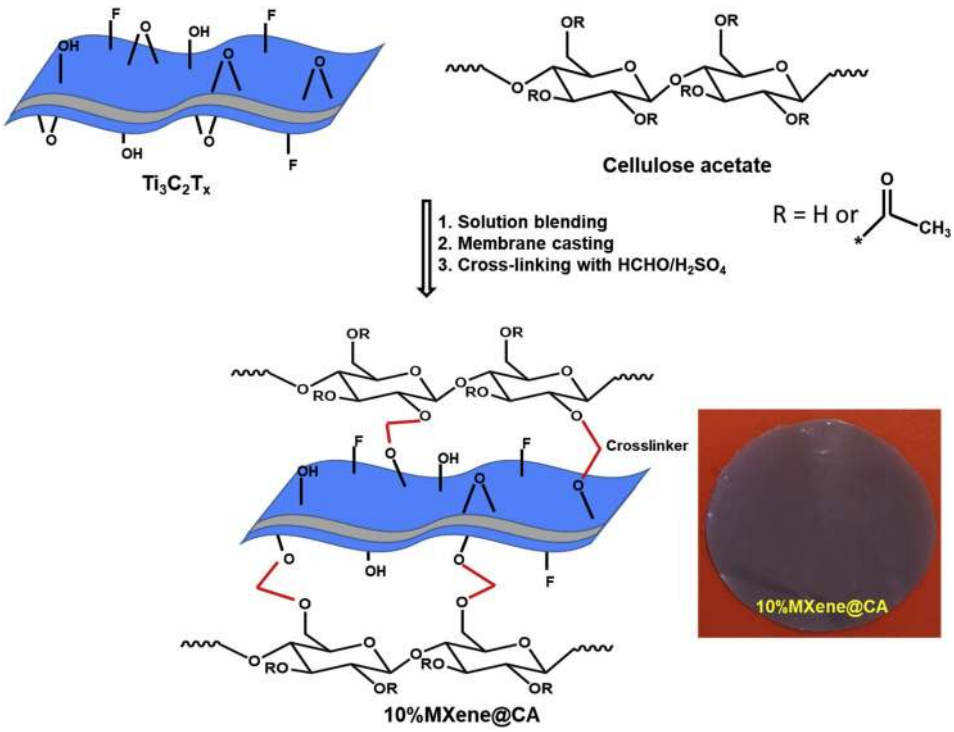

Scheme 1. Proposed reaction route for the synthesis of cross-linked MXene@CA hybrid nanoporous Membranes.

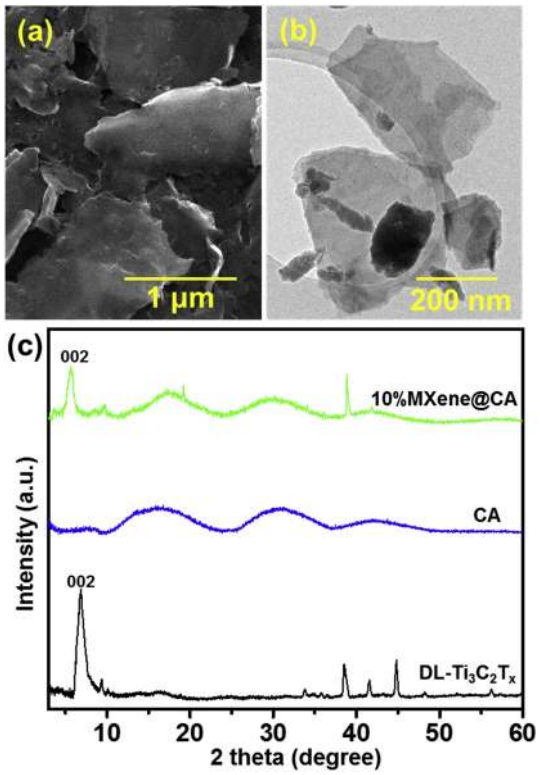

Fig. 1. (a) SEM image of DL-$Ti_3C_2T_x$, (b) TEM image of DL-$Ti_3C_2T_x$ and (c) XRD pattern of DL-$Ti_3C_2T_x$, CA and 10%MXene@CA Membrane.

~3.81 Å, and ~6.68 Å, respectively. The (002) peak shifts toward lower angles in 10%MXene@CA is most likely due to further dispersion of MXene sheets within the polymeric matrix [61]. This observation indicates the stable nature of MXene sheets between CA polymeric matrixes after cross-linking.

The surface and cross-section morphology of CA, CCA, 10%MXene/CA, and 10%MXene@CA membranes were studied by SEM. The surface morphology of pristine CA membranes exhibited microscale pores on the surface, and the cross-section shows spongy-like structures (Fig. 2(a and b)), respectively. After, chemical cross-linking of the pristine CA membrane, the surface became dense with observed nanopores (Fig. 2(c and d)). The surface and cross-sectional morphology of the 10%MXene/CA membrane before crosslinking exhibited a highly rough surface while maintaining the nonporous and sponge-like structure of CA (Fig. 2 (e and f)). On the other hand, surface and cross-sectional morphology of the 10%MXene@CA membrane turned to a dense with irregular arrangements of channels, most likely due to the chemical cross-linking between MXene and CA and condensation on MXene sheets in the channels [12]. The EDS spectrum and elemental mapping images (inserts) provide further evidence for the good dispersion of MXene sheets within the 10%MXene@CA membrane, as clearly observed from the uniform distribution of Ti element within the membrane matrix (Fig. S2).

The membrane hydrophilicity is elucidated by measuring the water contact angle. The lower value of the water contact angle is favored for high membrane hydrophilicity, which can attract more water molecules and thus improve the water flux and antifouling property of the membranes [62–64]. Water contact angles of the MXene ($Ti_3C_2T_x$), pristine CA, CCA, 10%MXene/CA, and 10%MXene@CA membranes are given in Fig. 3. The water contact angle have decreased from 70.3° of pristine CA to 54.0° for 10%MXene/CA with the incorporation of MXene, which is attributed to the excellent hydrophilic nature of MXene sheets and confirmed the improved membrane surface hydrophilicity. Water contact angle of pristine MXene was 41°. However, chemical cross-linking have led to a slight increase of water contact angle from 70.3° (Pristine CA) to 74.6° (CCA), and 54° (10%MXene/CA) to 60.8° (10%MXene@CA), most likely due to a decrease in the overall density of the hydroxyl groups as they get involved in the chemical cross-linking [65]. Overall, the hydrophilicity of the 10%MXene@CA membrane has been significantly improved by the incorporation of MXene.

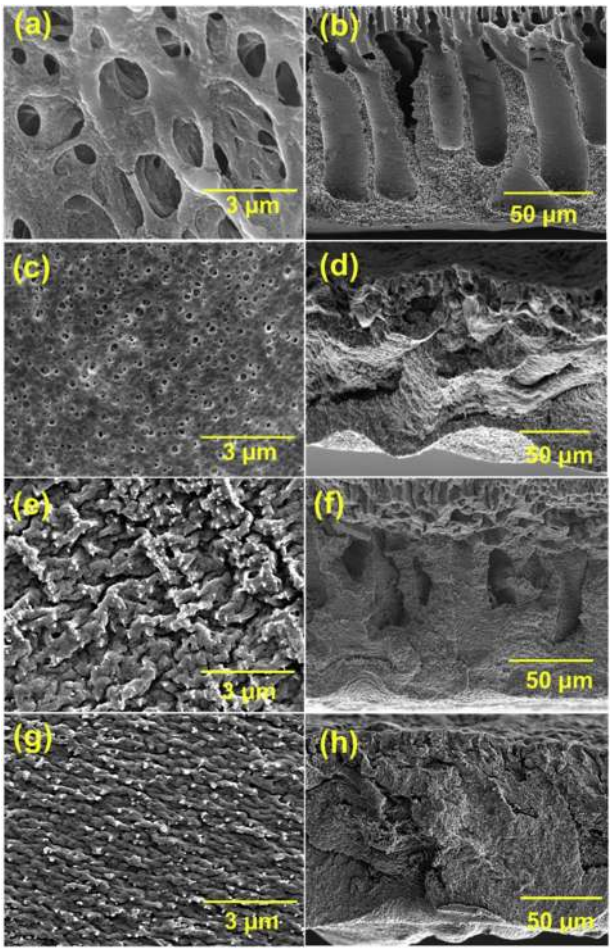

Fig. 2. SEM images: (a) CA membrane showing pores on the surface, (b) cross-section of CA, showing pore channels (c) CCA membrane, showing dense surface (d) cross-section of CCA, showing dense structure (e) surface of 10% MXene/CA, showing reduction in pore size after incorporation of MXene (f) cross-section of 10%MXene/CA, showing dense structure (g) 10%MXene@CA membrane, showing dense surface after crosslinking and (h) cross-section of 10%MXene@CA, showing dense structure throughout the membrane matrix.

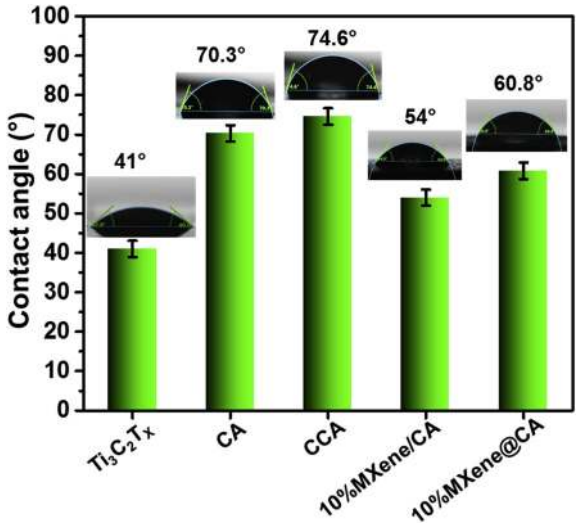

Fig. 3. Water contact angle of CA, CCA, 10%MXene/CA, and 10%MXene@CA membranes.

3.2. Chemical and thermal stability

Sodium hypochlorite is widely used as a disinfectant to meet drinking water standards. However, its strong oxidizing nature endangers membrane integrity under the standard operating conditions. Fig. 4 (a) showed the percentage weight loss of the prepared membranes after treatment with 0.1% aqueous solution of NaOCl for different time intervals (0–70 h). The 10%MXene@CA membrane exhibited highest chemical stability indicated by only 1.7% compared to 2.9% weight loss of pristine CA, most likely due to the incorporation of MXene together with chemical cross-linking. Notably, all composite membranes exhibited no appreciable weight loss after 45 h treatment. Fig. 4 (b) shows the TGA curves for CA, CCA, 10%MXene/CA, and 10%MXene@CA membranes. A three-step weight loss was observed. The first step at the temperature up to 150 °C, involved the release of absorbed and bound water present in the membrane matrix. Second step from 250 °C to 375 °C most likely involved the decomposition of oxygen-containing groups and polymer backbone. The third step might involve the decomposition of residual carbon from CA and MXene. The CA polymeric matrix started decomposition at 266 °C. The incorporation of MXene caused the most significant improvement of thermal stability of 10%MXene/CA, where the decomposition temperature shifted to 291 °C. Furthermore, chemical crosslinking enhanced the thermal stability of 10%MXene@CA composite, where decomposition shifted to ~300 °C, most likely due to the crosslinking of CA polymer backbone with MXene [66,67].

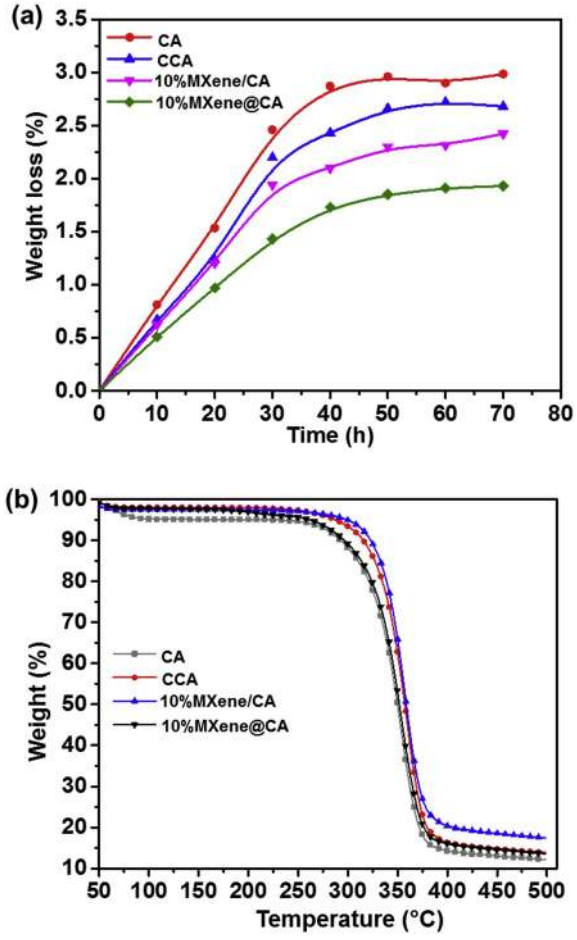

Fig. 4. (a) Oxidative stability of prepared composite membranes after treatment with 0.1% aqueous NaOCl solution at 70 °C for different time intervals (0–70 h), and (b) thermogravimetric analysis (TGA) of CA, CCA, 10%MXene/CA and 10%MXene@CA membranes.

3.3. Water uptake, membrane porosity, and surface charge characterization

Fig. 5 shows the water uptake (WU) and porosity of the prepared (0–10 wt%) MXene@CA composite membranes. The WU and porosity of the membranes are directly proportional to the presence of ionic clusters formed by hydrogen bonding and void volumes in the membrane matrix. Both have increased with the increase of MXene % loading. A linear trend was observed for all the cross-linked MXene@CA membranes with increasing the amount of MXene (Fig. 5 (a&b)). 10%MXene@CA showed 1.4 fold WU (123%) and 1.17 porosity (69.7%) in comparison with prepared CCA membrane 88.0%, 59.4% WUand porosity. Surface charges indicated by the zeta potential of CA and MXene@CA composite membranes were measured at pH = 7, as presented in Fig. S3. All CA and MXene@CA composite membranes exhibited negatively charged surface at pH 7, and the zeta potential value increased with the increase of MXene content. The 10%MXene@CA membrane had more negative zeta potential value (−32.42 mV) compare to pristine CA membrane (−24.84 mV) due to the negative surface of MXene sheets, leading to significant enhancement in the effective negative charge [68].

3.4. Membrane separation performance

After the successful preparation of CA, CCA, MXene/CA, and MXene@CA membranes, the effect of crosslinking and MXene content on the membrane separation performance were assessed in terms of pure water flux and rejection. The water flux of MXene@CA composite membranes have increased with increasing MXene content in the membrane (Fig. 6 (a)). The water flux has decreased with increasing crosslinking time from 30 to 120 min (Fig. S4), while rejection of Na_2SO_4 showed a pronounced increase from 30 to 60 min. After which, a slow rejection increase was observed with time (Fig. S5). Based on these results, 60 min was selected as the optimal crosslinking time in our further analysis. Fig. 6 (a) shows the pure water flux of the prepared pristine CA, CCA, MXene/CA and MXene@CA composite membranes. Incorporation of MXene in CA matrix has significantly improved the pure water flux, due to the formation of additional nanopores and hydrophilic nature of MXene. For 10%MXene/CA, water flux increased to 269.02 L m^{-2} bar^{-1} h^{-1}. However, after chemical cross-linking of 10%MXene@CA membrane, the flux has slightly decreased to 256.85 L m^{-2} bar^{-1} h^{-1}, as compared with 205 ± 6 L m^{-2} bar^{-1} h^{-1} the water flux of pristine CA membrane (Fig. 6 (a)). Overall, the pure water flux for the 10%MXene@CA composite membrane was improved as compared with the crosslinked CA membrane (CCA).

Solute rejection performance of CA, CCA, 10%MXene/CA, and MXene@CA composite membranes for different salts, dyes and BSA are given in Fig. 6(b–d). The rejection behavior of prepared membranes is believed to be a physical sieving phenomenon. The rejection values revealed the typical solute hydrated diameter related to the rejection performance. The 2%MXene@CA membrane crosslinked at 60 °C for 60 min exhibited a 3.28% rejection for Na_2SO_4, which was improved to 58.65% rejection using 10%MXene@CA membrane with the same crosslinking condition. The increase in rejection performance of MXene@CA membranes with increasing MXene content could be explained as the formation of denser layers as well as chemical cross-linking. The 10%MXene@CA membrane exhibited 28.14%, 40.35%, 56.08%, 92.34%, 98.27%, and 100% rejection for NaCl, $MgCl_2$, $MgSO_4$, RhB, MG and BSA, respectively. Meanwhile, bare CA membrane exhibited insignificant rejection for NaCl, $MgCl_2$, $MgSO_4$, Na_2SO_4, RhB, and MG, as well as 65.25% rejection for BSA. Incorporation of MXene into the CA matrix and the chemical cross-linking step have significantly improved the solute rejection as attributed to the formation of smaller pore diameter and decreased macrovoids (Fig. 6(c and d)). The reduction in water flux and improvement in solute rejection of 10%MXene@CA

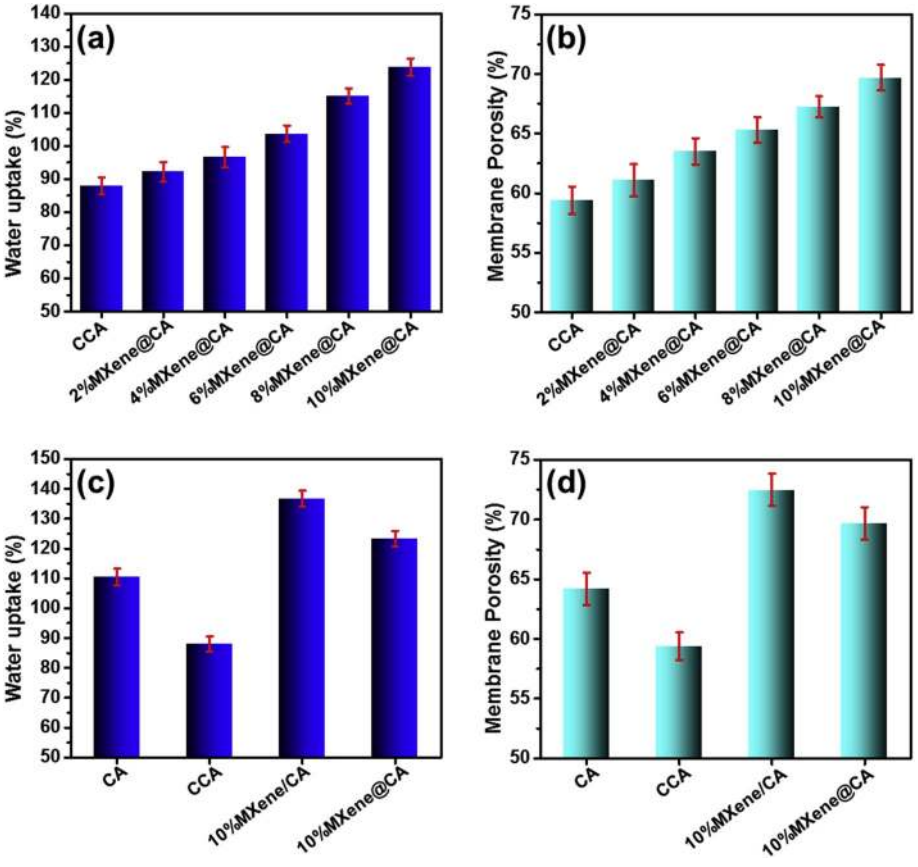

Fig. 5. Water uptake and membrane porosity of CA, CCA, and MXene@CA composite membranes.

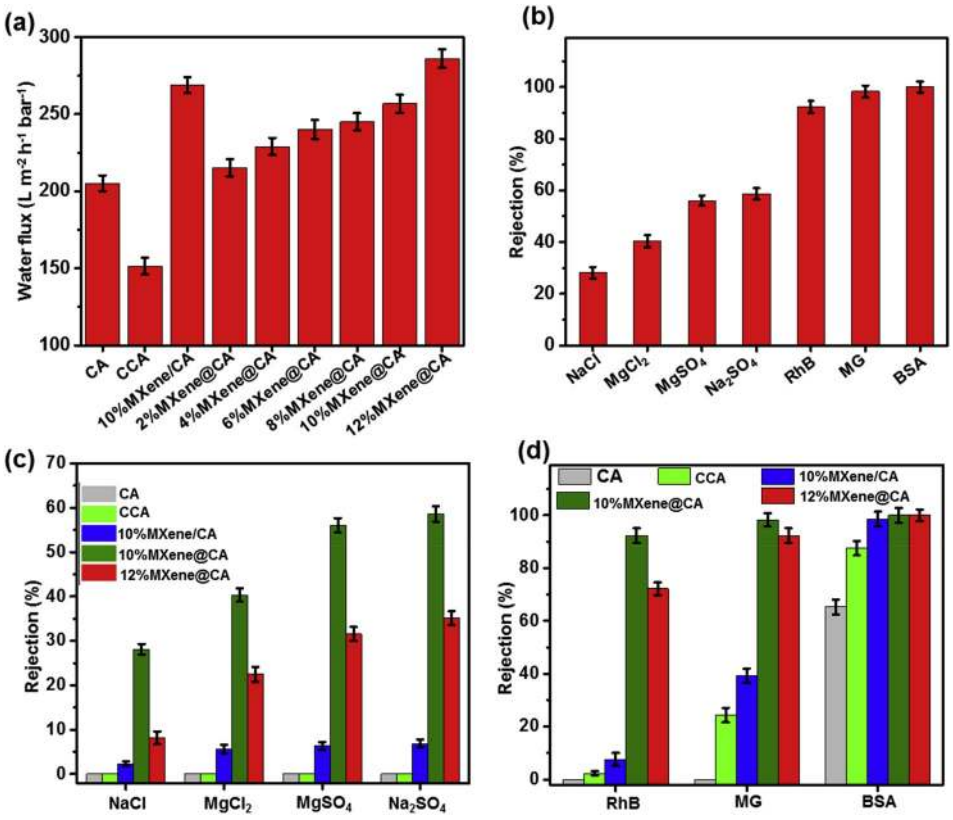

Fig. 6. (a) Pure water flux, (b) Rejection performance of the prepared 10%MXene@CA membrane (c) Comparison of rejection performance of CA, CCA, 10%MXene/CA, and 10%MXene@CA membranes for different salts, and (d) Comparison of rejection performance of CA, CCA, 10%MXene/CA, and 10%MXene@CA membranes for different dyes and protein.

membrane compared to 10%MXene/CA membrane was observed (Fig. 2). The water flux depends upon the density and size of pores and hydrophilic nature of the membranes, while the solute rejection depends upon the surface charge and pore size of the membranes. In the case of 10%MXene@CA membrane, chemical crosslinking leads to a reduction in the density and size of the membrane pores, while maintaining good hydrophilicity due to the dispersion of MXene within the polymeric matrix. Membranes with more than 10 wt% MXene loading lead to a small increase in the pure water flux, while a notable decrease in salt rejection, maybe due to the agglomeration of MXene at higher loadings. Thus, incorporation of MXene up to 10% loading has improved hydrophilicity and decreased pore diameter of the macrovoids. The pore diameter of the prepared MXene@CA composite membranes was calculated on the basis of solute rejection data, using above equation (5). The average uniform pore diameter of the 10%MXene/CA and 10% MXene@CA composite membranes were found to be 7.47 nm and 1.89 nm, respectively. The MWCO for 10%MXene@CA membrane, was estimated from the plot of rejection (%) of solute against their molecular weight in Daltons and given in Fig. S6. The MWCO of 10%MXene@CA membrane was found to be ~484 Da.

The membrane thickness also had a noticeable influence on the pure water flux and rejection performance of 10%MXene@CA membrane (Fig. S7). Pure water flux was decreased, while the rejection of Na_2SO_4 increased with increasing the membrane thickness. 10%MXene@CA membranes with thickness of 92, 123, 145, and 158 μm shows pure water flux of 293.94, 256.85, 221.18, and 178.31 L m^{-2} bar^{-1} h^{-1}, and rejection of Na_2SO_4 42.31%, 58.65%, 62.51%, and 65.28%, respectively. On the basis of the above results, 10%MXene@CA membrane with a thickness of 123 μm, was optimum for obtaining high separation performance. Table 1 proved the pure water flux and rejection of 10% MXene@CA composite membrane in comparison with previously reported cellulose acetate, MXene and GO composite membranes. The 10%MXene@CA composite membrane exhibited excellent separation performance, compared to reported membranes (Table 1).

3.5. *Effect of operating conditions on the separation performance of 10% MXene/CA and 10%MXene@CA membranes*

Effect of operating pressure and concentration of solute on the separation performance of 10%MXene/CA and 10%MXene@CA membranes were examined as described in Fig. 7. As expected, the pure water flux of 10%MXene/CA and 10%MXene@CA membranes was increased with increasing operating pressure, while the rejection of $MgSO_4$ has decreased (Fig. 7 (a)). The effect of concentration of $MgSO_4$ (2000–4000 ppm) on the separation performance of 10%MXene/CA and 10%MXene@CA membranes were studied and the results given in Fig. 7 (b). The rejection performance of both membranes have decreased with increasing the feed concentration of $MgSO_4$ from 2000 ppm to 4000 ppm, most likely due to the enhancement of the electrostatic shield effect due to the higher solute concentration [77].

3.6. *Flux recovery test*

Long-term durability of a membrane is critical for practical application with a controlled fouling rate. Fig. S8 showed the three-cycle filtration tests of 10%MXene@CA membrane with 0.1 g/L RhB solution at 1 bar. To study the durability and flux recovery, each cycle was carried out for 120 min. The 10%MXene@CA membrane was washed four times with DI water after each cycle to remove the adsorbed RhB. The water flux of 10%MXene@CA membrane has been decreased by 4.30% after three cycles (360 min) of RhB filtration. At the first cycle (120 min), the flux has decreased by 3.73%. After which, only 2.44% and 0.50% flux decreases were observed for the second and third cycles, respectively. Moreover, 10%MXene@CA membrane showed 97.56%,

Table 1
The performance of the prepared MXene@CA composite membranes compared with other reported cellulose acetate, MXene, and GO membranes.

Membrane	Salt/ Dye	Pure water flux (L m^{-2} h^{-1} bar^{-1})	Rejection (%)	Reference
GO@nylon 6-13	MB	11	95	[10]
	MO		99	
	NaCl		27	
	Na_2SO_4		56	
PA 6@GO (120)@ PA 6	MB	13	92	[7]
	MO		99	
GO/PDA/PSF	NaCl	81	19	[69]
	Na_2SO_4		46	
	MB		66	
	RhB		95	
G-CNTm	NaCl	11	51	[70]
	Na_2SO_4		83	
	MO		96	
GO-COOH	NaCl	5	48	[71]
	Na_2SO_4		91	
ATP/GO	RhB	41	99	[72]
CA/MOF@$GO_{0.12}$	BSA	122	~92	[26]
CNCs/CDA	BSA	75	90	[73]
CA/GO-0.5	BSA	125	90	[74]
GO-UR/CA	NaCl	20	27	[75]
	$MgSO_4$		73	
1.5% CGO	MO	30	53	[76]
	BSA		100	
CA:PA = 4:1	BSA	34	60	[28]
MXene membrane	RhB	1000	85	[34]
	BSA		100	
MXene ($Ti_3C_2T_x$)	RhB	118	81	[50]
	MG		94	
	BSA		100	
21% Ag@MXene	RhB	420	80	[50]
	MG		92	
	BSA		100	
10%MXene@CA	NaCl	256	28	This work
	$MgSO_4$		56	
	Na_2SO_4		59	
	RhB		92	
	MG		98	
	BSA		100	

Methylene blue (MB), Methyl orange (MO), Methyl green (MG), Rhodamine (RhB).

99.35%, and 99.57% flux recovery after first, second and third cycles filtration of RhB, respectively. This remarkable performance revealed the excellent durability and flux recovery of the prepared 10%MXene@CA membrane.

3.7. Antibacterial properties of the MXene@CA membranes

Antibacterial properties of the MXene@CA membranes were evaluated against *E. coli* and *B. subtilis* to estimate the anti-biofouling activity of the membranes. The cell viability was measured by counting the number of colonies and plotted in comparison with the CCA membrane as control. The photograph of *E. coli* and *B. subtilis* on the CCA, 2% MXene@CA, 6%MXene@CA, 8%MXene@CA, and 10%MXene@CA membranes at 35 °C for 24 h are given in Fig. 8. It is clearly visible that bacterial growth was inhibited in the presence of MXene in comparison with CCA membrane and the growth inhibition increases with the increasing concentration of MXene in the membranes. Fig. 9 shows the cell viability plot for both *E. coli* and *B. subtilis* grown on different MXene@CA composite membranes. The cell viability was decreased with increasing the MXene concentration. Membrane with the highest concentration (10%MXene@CA) exhibited more than 98% and 96% growth inhibition for *E. coli* and *B. subtilis*, as compared with CCA membrane, respectively. It was proved that $Ti_3C_2T_x$ having strong antibacterial activity against Gram-negative *E. coli* and Gram-positive *B. subtilis* bacteria and the activity was dose-dependent [38]. The possible mechanism of antibacterial activity can be proposed as the disruption of cellular membranes by sharp edges of the MXene nanosheets through direct contact-killing, leading to cell damage [41]. In addition, a three-step cytotoxicity mechanism for antibacterial activity of MXene nanosheets has been previously proposed [38]. The mechanism includes the adhesion of bacteria onto the membrane surface, followed by membrane disruptive interaction with bacteria that induces membrane stress. Finally the reaction between MXene sheet with some molecules in the cell wall/cytoplasm of the bacteria results in a disruption of the cell structure.

To evaluate the interaction of the membrane with bacteria, the morphological characterization of membrane surfaces after 24 h of incubation were compared by using SEM. Fig. 10 shows the SEM images of the CCA membrane and 10%MXene@CA membranes with *E. coli* and *B. subtilis* cells on the membrane's surface. As shown in Fig. 10(a) and (c), viable *E. coli* and *B. subtilis* cells were observed on the CCA membrane. On the other hand, no or minimal viable cells were observed on the 10%MXene@CA membranes for both *E. coli* and *B. subtilis* (Fig. 10(b) and (d). Moreover, the bacteria on the CCA membranes were very healthy without any damage. On the other hand, very few bacteria even with damages were present on the surface of 10%MXene@CA membrane.

3.8. Separation mechanism of 10%MXene@CA composite membrane

The significant separation performance of 10%MXene@CA composite membrane can be explained with its excellent physicochemical properties improved by the incorporation of 2D $Ti_3C_2T_X$ nanosheets. The water flux depends upon the density and size of pores and hydrophilic nature of the membranes. The wrinkled sheet-like flakes and highly hydrophilic $Ti_3C_2T_X$ permit more water molecules to entering through the membrane. Nanometers thin $Ti_3C_2T_X$ sheets provide 2D capillary network to accelerate water molecules through the membrane,

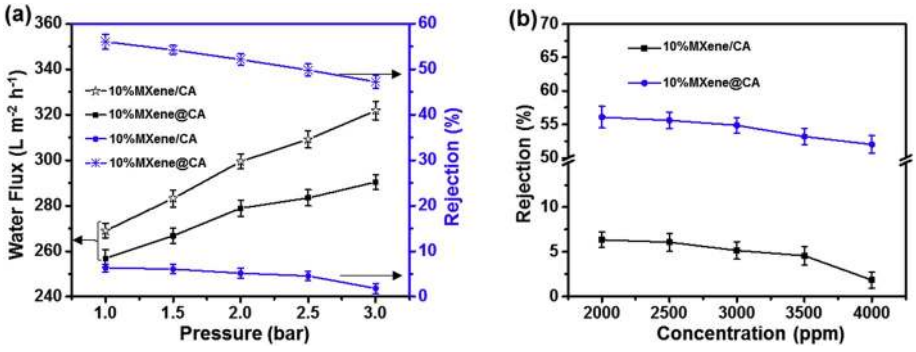

Fig. 7. (a) Effect of operating pressure on pure water flux and rejection of 2000 ppm of $MgSO_4$ and (b) effect of $MgSO_4$ concentration on rejection performance of 10%MXene/CA and 10%MXene@CA membranes.

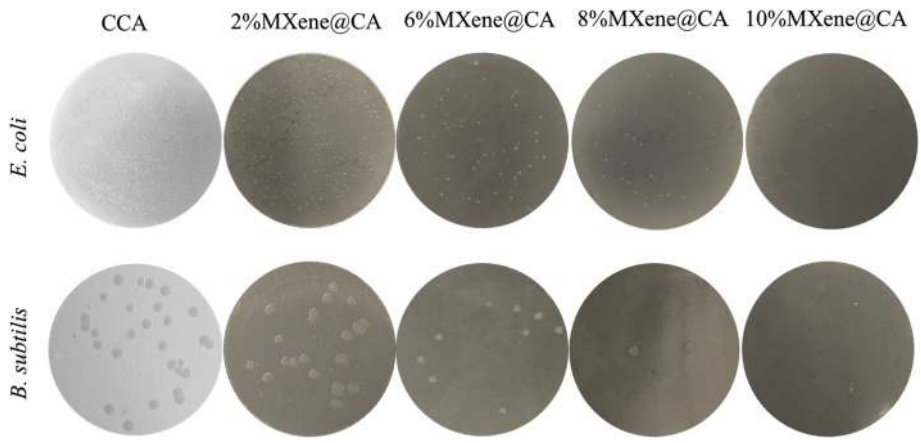

Fig. 8. Antibacterial activity of MXene@CA membranes: Photographs of *E. coli* and *B. subtilis* growth on different MXene@CA membranes incubated at 35 °C for 24 h.

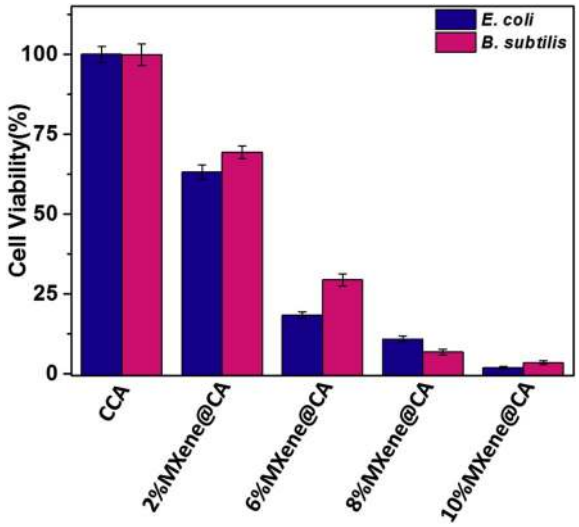

Fig. 9. Antibacterial activity of MXene@CA membranes: Cell viability measurements (by colony forming count method) of *E. coli* and *B. subtilis* on different MXene@CA membranes 24 h. Error bars represent the standard deviation of triplicate experiments.

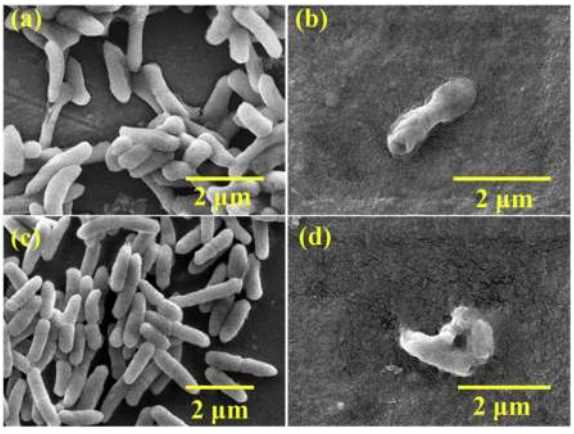

Fig. 10. SEM images: (a) *E. coli* cells grown on CCA membrane (b) *E. coli* cells grown on 10%MXene@CA membrane (c) *B. subtilis* cells grown on CCA membrane and (d) *B. subtilis* cells grown on 10%MXene@CA membrane.

subsequently increase the water flux compared to bare CA. Water contact angle has decreased from 70.3° to 60.8° with incorporation of $Ti_3C_2T_X$ content from 0 to 10% in the CA matrix and confirmed that the hydrophilicity of 10%MXene@CA membrane have increased. The solute rejection depends upon the surface charge and pore size of the membranes. Incorporation of MXene into the CA matrix and chemical cross-linking significantly improves the solute rejection compare to the bare CA membrane, most likely due to the formation of smaller pore diameter and decreased macrovoids. The large salt and dye molecules are directly rejected due to the size exclusion. Moreover, $Ti_3C_2T_X$ acts as the antimicrobial agent in the membrane matrix, thus improving antibiofouling properties of 10%MXene@CA membrane.

4. Conclusions

In conclusion, we have successfully fabricated chemically cross-linked MXene@CA composite membranes by a facile solution blending followed by chemical cross-linking. Prepared MXene@CA composite membrane, especially 10%MXene@CA cross-linked at 60 °C for 60 min, showed excellent hydrophilicity, high water uptake, biofouling resistance, and chlorine tolerant nature. Pore diameter (~1.89 nm) and separation performance of the prepared 10%MXene@CA membrane revealed their suitability for water treatment. 10%MXene@CA membrane showed a highly competitive separation performance of as compared with reported CA, GO, and MXene membranes in the literature. The 10%MXene@CA membrane showed highly efficient bactericidal properties against *E. coli* and *B. subtilis*, indicating the strong antibiofouling performance of the MXene-enforced membrane. These results will open the door for high performance and cost effective UF/NF membranes based on MXene composites.

Declaration of competing interest

There are no conflicts to declare.

Acknowledgments

RP, and PAR acknowledge the financial support of Qatar National Research Fund (A member of Qatar Foundation) through the National Priorities Research Program (NPRP) grants (# 9-254-2-120), and (#8-286-2-118). The authors are thankful to A. R. Shetty, A. Samara, M. Pasha, and M. Helal at the Core lab of QEERI/HBKU, Qatar, for XRD, water contact angle, and SEM analysis and K. A. Jabbar, QEERI for the support with bactericidal studies. The publication of this article was funded by the Qatar National Library.

Appendix A. Supplementary data

Supplementary data to this article can be found online at https://doi.org/10.1016/j.memsci.2020.118139.

References

[1] M. Safarpour, V. Vatanpour, A. Khataee, Preparation and characterization of graphene oxide/TiO2 blended PES nanofiltration membrane with improved antifouling and separation performance, Desalination 393 (2016) 65–78.
[2] M. Peydayesh, T. Mohammadi, O. Bakhtiari, Water desalination via novel positively charged hybrid nanofiltration membranes filled with hyperbranched polyethyleneimine modified MWCNT, J. Ind. Eng. Chem. 69 (2019) 127–140.
[3] Y. Zhao, Z. Zhang, L. Dai, S. Zhang, Preparation of a highly permeable nanofiltration membrane using a novel acyl chloride monomer with -PO(Cl)2 group, Desalination 431 (2018) 56–65.
[4] M. Guo, S. Wang, K. Gu, X. Song, Y. Zhou, C. Gao, Gradient cross-linked structure: towards superior PVA nanofiltration membrane performance, J. Membr. Sci. 569 (2019) 83–90.
[5] Y.-F. Mi, F.-Y. Zhao, Y.-S. Guo, X.-D. Weng, C.-C. Ye, Q.-F. An, Constructing zwitterionic surface of nanofiltration membrane for high flux and antifouling performance, J. Membr. Sci. 541 (2017) 29–38.
[6] S. Sarkar, A.K. SenGupta, P. Prakash, The donnan membrane principle: opportunities for sustainable engineered processes and materials, Environ. Sci. Technol. 44 (2010) 1161–1166.
[7] L. Chen, N. Li, Z. Wen, L. Zhang, Q. Chen, L. Chen, P. Si, J. Feng, Y. Li, J. Lou, L. Ci, Graphene oxide based membrane intercalated by nanoparticles for high performance nanofiltration application, Chem. Eng. J. 347 (2018) 12–18.
[8] G. Liu, W. Jin, N. Xu, Graphene-based membranes, Chem. Soc. Rev. 44 (2015) 5016–5030.
[9] N. Wang, S. Ji, G. Zhang, J. Li, L. Wang, Self-assembly of graphene oxide and polyelectrolyte complex nanohybrid membranes for nanofiltration and pervaporation, Chem. Eng. J. 213 (2012) 318–329.
[10] L. Chen, Y. Li, L. Chen, N. Li, C. Dong, Q. Chen, B. Liu, Q. Ai, P. Si, J. Feng, L. Zhang, J. Suhr, J. Lou, L. Ci, A large-area free-standing graphene oxide multilayer membrane with high stability for nanofiltration applications, Chem. Eng. J. 345 (2018) 536–544.
[11] A.K. Singh, P. Singh, S. Mishra, V.K. Shahi, Anti-biofouling organic-inorganic hybrid membrane for water treatment, J. Mater. Chem. 22 (2012) 1834–1844.
[12] A.K. Singh, S. Prakash, V. Kulshrestha, V.K. Shahi, Cross-linked hybrid nanofiltration membrane with antibiofouling properties and self-assembled layered morphology, ACS Appl. Mater. Interfaces 4 (2012) 1683–1692.
[13] B.P. Tripathi, N.C. Dubey, M. Stamm, Polyethylene glycol cross-linked sulfonated polyethersulfone based filtration membranes with improved antifouling tendency, J. Membr. Sci. 453 (2014) 263–274.
[14] M. Paul, S.D. Jons, Chemistry and fabrication of polymeric nanofiltration membranes: a review, Polymer 103 (2016) 417–456.
[15] H. Abadikhah, E. Naderi Kalali, S. Khodi, X. Xu, S. Agathopoulos, Multifunctional thin-film nanofiltration membrane incorporated with reduced graphene oxide@TiO2@Ag nanocomposites for high desalination performance, dye retention, and antibacterial properties, ACS Appl. Mater. Interfaces 11 (2019) 23535–23545.
[16] Z. Wang, Z. Wang, S. Lin, H. Jin, S. Gao, Y. Zhu, J. Jin, Nanoparticle-templated nanofiltration membranes for ultrahigh performance desalination, Nat. Commun. 9 (2018) 2004.
[17] H. Abadikhah, E.N. Kalali, S. Behzadi, S.A. Khan, X. Xu, M.E. Shabestari, S. Agathopoulos, High flux thin film nanocomposite membrane incorporated with functionalized TiO2@reduced graphene oxide nanohybrids for organic solvent nanofiltration, Chem. Eng. Sci. 204 (2019) 99–109.
[18] E. Bagheripour, A.R. Moghadassi, S.M. Hosseini, B. Van der Bruggen, F. Parvizian, Novel composite graphene oxide/chitosan nanoplates incorporated into PES based nanofiltration membrane: chromium removal and antifouling enhancement, J. Ind. Eng. Chem. 62 (2018) 311–320.
[19] A. Anand, B. Unnikrishnan, J.-Y. Mao, H.-J. Lin, C.-C. Huang, Graphene-based nanofiltration membranes for improving salt rejection, water flux and antifouling–A review, Desalination 429 (2018) 119–133.
[20] J. Zheng, M. Li, K. Yu, J. Hu, X. Zhang, L. Wang, Sulfonated multiwall carbon nanotubes assisted thin-film nanocomposite membrane with enhanced water flux and anti-fouling property, J. Membr. Sci. 524 (2017) 344–353.
[21] G. Dong, H. Li, V. Chen, Challenges and opportunities for mixed-matrix membranes for gas separation, J. Mater. Chem. 1 (2013) 4610–4630.
[22] F. Liu, N.A. Hashim, Y. Liu, M.R.M. Abed, K. Li, Progress in the production and modification of PVDF membranes, J. Membr. Sci. 375 (2011) 1–27.
[23] H. Karimnezhad, A.H. Navarchian, T. Tavakoli Gheinani, S. Zinadini, Incorporation of iron oxyhydroxide nanoparticles in polyacrylonitrile nanofiltration membrane for improving water permeability and antifouling property, React. Funct. Polym. 135 (2019) 77–93.
[24] M.T. Tsehaye, J. Wang, J. Zhu, S. Velizarov, B. Van der Bruggen, Development and characterization of polyethersulfone-based nanofiltration membrane with stability to hydrogen peroxide, J. Membr. Sci. 550 (2018) 462–469.
[25] C. Wei, Z. He, L. Lin, Q. Cheng, K. Huang, S. Ma, L. Chen, Negatively charged polyimide nanofiltration membranes with high selectivity and performance stability by optimization of synergistic imidization, J. Membr. Sci. 563 (2018) 752–761.
[26] S. Yang, Q. Zou, T. Wang, L. Zhang, Effects of GO and MOF@GO on the permeation and antifouling properties of cellulose acetate ultrafiltration membrane, J. Membr. Sci. 569 (2019) 48–59.
[27] B. Han, D. Zhang, Z. Shao, L. Kong, S. Lv, Preparation and characterization of cellulose acetate/carboxymethyl cellulose acetate blend ultrafiltration membranes, Desalination 311 (2013) 80–89.
[28] S.-s. Shen, H. Chen, R.-h. Wang, W. Ji, Y. Zhang, R. Bai, Preparation of antifouling cellulose acetate membranes with good hydrophilic and oleophobic surface properties, Mater. Lett. 252 (2019) 1–4.
[29] C.S. Ong, P.S. Goh, W.J. Lau, N. Misdan, A.F. Ismail, Nanomaterials for biofouling and scaling mitigation of thin film composite membrane: a review, Desalination 393 (2016) 2–15.
[30] J. Zhu, J. Hou, Y. Zhang, M. Tian, T. He, J. Liu, V. Chen, Polymeric antimicrobial membranes enabled by nanomaterials for water treatment, J. Membr. Sci. 550 (2018) 173–197.
[31] S. Beisl, S. Monteiro, R. Santos, A.S. Figueiredo, M.G. Sánchez-Loredo, M.A. Lemos, F. Lemos, M. Minhalma, M.N. de Pinho, Synthesis and bactericide activity of nanofiltration composite membranes – cellulose acetate/silver nanoparticles and cellulose acetate/silver ion exchanged zeolites, Water Res. 149 (2019) 225–231.
[32] S.M. Ghaseminezhad, M. Barikani, M. Salehirad, Development of graphene oxide-cellulose acetate nanocomposite reverse osmosis membrane for seawater desalination, Compos. B Eng. 161 (2019) 320–327.
[33] B. Anasori, M.R. Lukatskaya, Y. Gogotsi, 2D metal carbides and nitrides (MXenes) for energy storage, Nat. Rev. Mater. 2 (2017), 16098.
[34] L. Ding, Y. Wei, Y. Wang, H. Chen, J. Caro, H. Wang, A two-dimensional lamellar membrane: MXene nanosheet stacks, Angew. Chem. Int. Ed. 56 (2017) 1825–1829.
[35] R.P. Pandey, K. Rasool, P. Abdul Rasheed, K.A. Mahmoud, Reductive sequestration of toxic bromate from drinking water using lamellar two-dimensional Ti3C2TX (MXene), ACS Sustain. Chem. Eng. 6 (2018) 7910–7917.
[36] O. Mashtalir, M.R. Lukatskaya, M.-Q. Zhao, M.W. Barsoum, Y. Gogotsi, Amine-assisted delamination of Nb2C MXene for Li-ion energy storage devices, Adv. Mater. 27 (2015) 3501–3506.
[37] Y. Dall'Agnese, P.-L. Taberna, Y. Gogotsi, P. Simon, Two-Dimensional vanadium carbide (MXene) as positive electrode for sodium-ion capacitors, J. Phys. Chem. Lett. 6 (2015) 2305–2309.
[38] K. Rasool, M. Helal, A. Ali, C.E. Ren, Y. Gogotsi, K.A. Mahmoud, Antibacterial activity of Ti3C2Tx MXene, ACS Nano 10 (2016) 3674–3684.
[39] K. Rasool, R.P. Pandey, P.A. Rasheed, S. Buczek, Y. Gogotsi, K.A. Mahmoud, Water treatment and environmental remediation applications of two-dimensional metal carbides (MXenes), Mater. Today 30 (2019) 80–102.
[40] B.-M. Jun, S. Kim, J. Heo, C.M. Park, N. Her, M. Jang, Y. Huang, J. Han, Y. Yoon, Review of MXenes as new nanomaterials for energy storage/delivery and selected environmental applications, Nano Research 12 (2019) 471–487.
[41] X.-J. Zha, X. Zhao, J.-H. Pu, L.-S. Tang, K. Ke, R.-Y. Bao, L. Bai, Z.-Y. Liu, M.-B. Yang, W. Yang, Flexible anti-biofouling MXene/cellulose fibrous membrane for sustainable solar-driven water purification, ACS Appl. Mater. Interfaces 11 (2019) 36589–36597.
[42] M. Naguib, M. Kurtoglu, V. Presser, J. Lu, J. Niu, M. Heon, L. Hultman, Y. Gogotsi, M.W. Barsoum, Two-Dimensional nanocrystals produced by exfoliation of Ti3AlC2, Adv. Mater. 23 (2011) 4248–4253.
[43] M. Ghidiu, M.R. Lukatskaya, M.-Q. Zhao, Y. Gogotsi, M.W. Barsoum, Conductive two-dimensional titanium carbide 'clay' with high volumetric capacitance, Nature 516 (2014) 78.
[44] M. Alhabeb, K. Maleski, B. Anasori, P. Lelyukh, L. Clark, S. Sin, Y. Gogotsi, Guidelines for synthesis and processing of two-dimensional titanium carbide (Ti3C2Tx MXene), Chem. Mater. 29 (2017) 7633–7644.
[45] K. Maleski, V.N. Mochalin, Y. Gogotsi, Dispersions of two-dimensional titanium carbide MXene in organic solvents, Chem. Mater. 29 (2017) 1632–1640.
[46] R. Han, X. Ma, Y. Xie, D. Teng, S. Zhang, Preparation of a new 2D MXene/PES composite membrane with excellent hydrophilicity and high flux, RSC Adv. 7 (2017) 56204–56210.
[47] C.E. Ren, K.B. Hatzell, M. Alhabeb, Z. Ling, K.A. Mahmoud, Y. Gogotsi, Charge- and size-selective ion sieving through Ti3C2Tx MXene membranes, J. Phys. Chem. Lett. 6 (2015) 4026–4031.
[48] X. Wu, L. Hao, J. Zhang, X. Zhang, J. Wang, J. Liu, Polymer-Ti3C2Tx composite membranes to overcome the trade-off in solvent resistant nanofiltration for alcohol-based system, J. Membr. Sci. 515 (2016) 175–188.
[49] K. Rasool, K.A. Mahmoud, D.J. Johnson, M. Helal, G.R. Berdiyorov, Y. Gogotsi, Efficient antibacterial membrane based on two-dimensional Ti3C2Tx (MXene) nanosheets, Sci. Rep. 7 (2017) 1598.
[50] R.P. Pandey, K. Rasool, V.E. Madhavan, B. Aïssa, Y. Gogotsi, K.A. Mahmoud, Ultrahigh-flux and fouling-resistant membranes based on layered silver/MXene (Ti3C2Tx) nanosheets, J. Mater. Chem. 6 (2018) 3522–3533.
[51] G. Liu, J. Shen, Q. Liu, G. Liu, J. Xiong, J. Yang, W. Jin, Ultrathin two-dimensional MXene membrane for pervaporation desalination, J. Membr. Sci. 548 (2018) 548–558.
[52] K.M. Kang, D.W. Kim, C.E. Ren, K.M. Cho, S.J. Kim, J.H. Choi, Y.T. Nam, Y. Gogotsi, H.-T. Jung, Selective molecular separation on Ti3C2tx–graphene oxide membranes during pressure-driven filtration: comparison with graphene oxide and MXenes, ACS Appl. Mater. Interfaces 9 (2017) 44687–44694.
[53] S. Wei, Y. Xie, Y. Xing, L. Wang, H. Ye, X. Xiong, S. Wang, K. Han, Two-dimensional graphene Oxide/MXene composite lamellar membranes for efficient solvent permeation and molecular separation, J. Membr. Sci. 582 (2019) 414–422.
[54] R. Han, Y. Xie, X. Ma, Crosslinked P84 copolyimide/MXene mixed matrix membrane with excellent solvent resistance and permselectivity, Chin. J. Chem. Eng. 27 (2019) 877–883.

[55] Z. Xu, G. Liu, H. Ye, W. Jin, Z. Cui, Two-dimensional MXene incorporated chitosan mixed-matrix membranes for efficient solvent dehydration, J. Membr. Sci. 563 (2018) 625–632.
[56] R.P. Pandey, A.K. Thakur, V.K. Shahi, Stable and efficient composite anion-exchange membranes based on silica modified poly(ethyleneimine)–poly(vinyl alcohol) for electrodialysis, J. Membr. Sci. 469 (2014) 478–487.
[57] A.K. Singh, R.P. Pandey, A. Jasti, V.K. Shahi, Self-assembled silica nanocrystal-based anti-biofouling nanofilter membranes, RSC Adv. 3 (2013) 458–467.
[58] A.K. Singh, S. Prakash, V. Kulshrestha, V.K. Shahi, Cross-linked hybrid nanofiltration membrane with antibiofouling properties and self-assembled layered morphology, ACS Appl. Mater. Interfaces 4 (2012) 1683–1692.
[59] B.P. Tripathi, V.K. Shahi, Organic–inorganic nanocomposite polymer electrolyte membranes for fuel cell applications, Prog. Polym. Sci. 36 (2011) 945–979.
[60] R.P. Pandey, A.K. Thakur, V.K. Shahi, Stable and efficient composite anion-exchange membranes based on silica modified poly(ethyleneimine)–poly(vinyl alcohol) for electrodialysis, J. Membr. Sci. 469 (2014) 478–487.
[61] Z. Ling, C.E. Ren, M.-Q. Zhao, J. Yang, J.M. Giammarco, J. Qiu, M.W. Barsoum, Y. Gogotsi, Flexible and conductive MXene films and nanocomposites with high capacitance, Proc. Natl. Acad. Sci. Unit. States Am. 111 (2014) 16676–16681.
[62] K. Chen, C. Xiao, Q. Huang, H. Liu, Y. Tang, Fabrication and properties of graphene oxide-embedded cellulose triacetate RO composite membrane via melting method, Desalination 425 (2018) 175–184.
[63] J. Lv, G. Zhang, H. Zhang, F. Yang, Graphene oxide-cellulose nanocrystal (GO-CNC) composite functionalized PVDF membrane with improved antifouling performance in MBR: behavior and mechanism, Chem. Eng. J. 352 (2018) 765–773.
[64] K.G. Zhou, K.S. Vasu, C.T. Cherian, M. Neek-Amal, J.C. Zhang, H. Ghorbanfekr-Kalashami, K. Huang, O.P. Marshall, V.G. Kravets, J. Abraham, Y. Su, A. N. Grigorenko, A. Pratt, A.K. Geim, F.M. Peeters, K.S. Novoselov, R.R. Nair, Electrically controlled water permeation through graphene oxide membranes, Nature 559 (2018) 236–240.
[65] L. Jin, Z. Wang, S. Zheng, B. Mi, Polyamide-crosslinked graphene oxide membrane for forward osmosis, J. Membr. Sci. 545 (2018) 11–18.
[66] S.-l. Yang, Z.-H. Wu, W. Yang, M.-B. Yang, Thermal and mechanical properties of chemical crosslinked polylactide (PLA), Polym. Test. 27 (2008) 957–963.
[67] Y. Zhan, X. Yang, H. Guo, J. Yang, F. Meng, X. Liu, Cross-linkable nitrile functionalized graphene oxide/poly(arylene ether nitrile) nanocomposite films with high mechanical strength and thermal stability, J. Mater. Chem. 22 (2012) 5602–5608.
[68] G. Liu, J. Zou, Q. Tang, X. Yang, Y. Zhang, Q. Zhang, W. Huang, P. Chen, J. Shao, X. Dong, Surface modified Ti3C2 MXene nanosheets for tumor targeting photothermal/photodynamic/chemo synergistic therapy, ACS Appl. Mater. Interfaces 9 (2017) 40077–40086.
[69] M. Hu, B. Mi, Enabling graphene oxide nanosheets as water separation membranes, Environ. Sci. Technol. 47 (2013) 3715–3723.
[70] Y. Han, Y. Jiang, C. Gao, High-flux graphene oxide nanofiltration membrane intercalated by carbon nanotubes, ACS Appl. Mater. Interfaces 7 (2015) 8147–8155.
[71] Y. Yuan, X. Gao, Y. Wei, X. Wang, J. Wang, Y. Zhang, C. Gao, Enhanced desalination performance of carboxyl functionalized graphene oxide nanofiltration membranes, Desalination 405 (2017) 29–39.
[72] Z. Luo, Q. Fang, X. Xu, D.V. Raj, X. Zhou, Z. Liu, Attapulgite nanofibers and graphene oxide composite membrane for high-performance molecular separation, J. Colloid Interface Sci. 545 (2019) 276–281.
[73] J. Lv, G. Zhang, H. Zhang, F. Yang, Exploration of permeability and antifouling performance on modified cellulose acetate ultrafiltration membrane with cellulose nanocrystals, Carbohydr. Polym. 174 (2017) 190–199.
[74] S. Vetrivel, M.S.A. Saraswathi, D. Rana, A. Nagendran, Fabrication of cellulose acetate nanocomposite membranes using 2D layered nanomaterials for macromolecular separation, Int. J. Biol. Macromol. 107 (2018) 1607–1612.
[75] Y. Zhang, K. Su, Z. Li, Graphene oxide composite membranes cross-linked with urea for enhanced desalting properties, J. Membr. Sci. 563 (2018) 718–725.
[76] Y. Jiang, Q. Zeng, P. Biswas, J.D. Fortner, Graphene oxides as nanofillers in polysulfone ultrafiltration membranes: Shape matters, J. Membr. Sci. 581 (2019) 453–461.
[77] Y.-S. Guo, Y.-L. Ji, B. Wu, N.-X. Wang, M.-J. Yin, Q.-F. An, C.-J. Gao, High-flux zwitterionic nanofiltration membrane constructed by in-situ introduction method for monovalent salt/antibiotics separation, J. Membr. Sci. 593 (2020), 117441.